Journal of Building Engineering 90 (2024) 109405

Contents lists available at ScienceDirect

Journal of Building Engineering

journal homepage: www.elsevier.com/locate/jobe

Effect of three-dimensional space on progressive collapse resistance of reinforced concrete frames under various column removal scenarios

Fei-Fan Feng [a], Hyeon-Jong Hwang [b,*], Yun Zhou [c,**], Jing-Ming Sun [c], Hu-Zhi Zhang [a], Jun-Ho Roh [b], Su-Min Kang [d], Wei-Jian Yi [c]

[a] School of Civil Engineering, Hunan University of Science and Technology, Xiangtan, 411201, China
[b] School of Architecture, Konkuk University, 05029, Seoul, South Korea
[c] College of Civil Engineering, Hunan University, Changsha, 410082, China
[d] School of Architecture, Soongsil University, Sangdo-dong, Seoul, 08826, South Korea

ARTICLE INFO

Keywords:
Numerical analysis
Reinforced concrete
Moment frame
Progressive collapse
3D spatial effect
Column removal scenarios

ABSTRACT

In this study, high fidelity finite element (FE) model was adopted to investigate the progressive collapse resistance of reinforced concrete (RC) frame structures under various column removal scenarios. The validity of the numerical model was verified by comparing with the existing experimental results. Afterwards, to facilitate the research on possible simplified boundary conditions served for further various column removal scenarios, the effect of multi-span continuous beams was firstly evaluated and the simplified methods were compared. Then, the effect of various column removal scenarios addressing the three-dimensional effect on the progressive collapse resistance of RC frame structures with and without slab was systematically evaluated. The analysis results showed that the continuous span beams increased the internal compressive force of the beam section at compressive arch action (CAA) stage, which effectively improved the CAA strength of the substructure. For simple modeling, the use of horizontal constraints at the end of the beam could replace the continuous span beams. The presence of transverse beams and slab provided additional load transfer paths for collapse resistance. The compressive membrane action (CMA) and tensile membrane action (TMA) of the slab significantly improved the progressive collapse resistance of the substructure in the small and large deformation stages, respectively. The location of the removed column significantly affected the contribution ratio of transverse beams and slab to the progressive collapse resistance of the substructure, which was quantitatively evaluated for practical design.

1. Introduction

In history, progressive collapse of building structures is always accompanied by serious casualties and property losses. All types of public and private buildings can be affected by extreme events, which often cause localized damage to the structure, resulting in partial

* Corresponding author.
** Co-corresponding author.
E-mail addresses: fengfeifan@hnust.edu.cn (F.-F. Feng), hwanggun85@naver.com, hwanghj@konkuk.ac.kr (H.-J. Hwang), zhouyun05@hnu.edu.cn (Y. Zhou), sunjingming@hnu.edu.cn (J.-M. Sun), zhanghz_hnu@163.com (H.-Z. Zhang), rjh1222@konkuk.ac.kr (J.-H. Roh), kangsm@ssu.ac.kr (S.-M. Kang), wjyi@hnu.edu.cn (W.-J. Yi).

https://doi.org/10.1016/j.jobe.2024.109405
Received 22 December 2023; Received in revised form 16 April 2024; Accepted 18 April 2024
Available online 22 April 2024

or even overall structural collapse [1,2]. Major accidents (e.g., progressive collapse of Ronan Point apartment in London in 1968, car bomb incident at Alfred P. Murrah Federal Building in 1995, and 911 terrorist attack in 2001) triggered widespread attention of the engineering and academic communities on the progressive collapse problems of building structures. Since then, many countries included the provisions related to this issue in design codes, and the design guidelines for structures against progressive collapse [3–5] have been released successively.

In general, since it is difficult to predict the probability and severity of extreme events, it is neither economical nor practical to design structures to deal with extreme events through traditional methods. The current anti-collapse design concepts mainly include direct and indirect design methods. As a direct design method, the alternative load path (ALP) method evaluates whether the structure can provide effective alternative load transfer path under ideal column removal scenarios. Considering the unpredictability of accidental events, this threat-independent design method is recognized as the most reliable method to evaluate the progressive collapse resistance of building structures. For this reason, the ALP method is adopted in this study.

In the last two decades, a large number of experimental studies on the progressive collapse resistance of RC/PC structures have been conducted [6]. The existing studies focused on the beam-column substructures [7–15], beam-slab substructures [16–22], and multi-story frame structures [23–29]. In general, the compressive arch action (CAA) and catenary action (CTA) in beams, as well as the compressive membrane action (CMA) and tensile membrane action (TMA) in slabs, provided additional progressive collapse resistance to the structures. The newly proposed multi-hazard resistant prefabricated frame structure systems [30–32] improved the resilience under both seismic and progressive collapse conditions. Further, various analytical models have been proposed to predict the progressive collapse resistance mechanisms of substructures, including the calculation methods for CAA [33–35], CTA [36–38], and membrane action of slab [39]. In general, each model could provide good prediction accuracy under the premise of satisfying its own characteristics. Also, efficient finite element (FE) methods were adopted for numerical studies to evaluate the progressive collapse performance of RC substructures [40–43], and the anti-explosion performance of RC frame buildings [44]. The progressive collapse process of the whole RC structures was also investigated based on the novel hybrid framework of FE method-physics engine [45].

However, progressive collapse tests are usually time-consuming and laborious, and the number of tests are limited. For this reason, the effect of design parameters on the progressive collapse resistance of building structures has not been completely evaluated, especially when various column removal scenarios are considered within the same three-dimensional building structures with and without slab, under the premise of reasonable consideration of boundary conditions. Similarly, under such conditions, simplified analysis models have the same limitations. Although existing numerical analysis studies have investigated the progressive collapse resistance of the frame and flat slab substructures, they usually focused on a specific column removal scenario without consideration of various column removal scenarios. Further, the contribution of slab to the progressive collapse resistance under various column removal scenarios needs to be evaluated. Thus, it is necessary to propose an accurate numerical simulation method to systematically evaluate the progressive collapse resistance of three-dimensional frame structures.

In the present study, LS-DYNA was adopted to conduct numerical analysis based on high fidelity FE models. The FE models were verified by comparing with the existing test results. Afterwards, to facilitate the study on possible simplified boundary conditions served for further various column removal scenarios, the effect of multi-span continuous beams was firstly evaluated and the simplified methods were compared. Then, with reasonable consideration of the boundary conditions, the effect of various column removal scenarios addressing the three-dimensional effect on the progressive collapse resistance of RC frame structures with and without slab was systematically evaluated, and the contribution of slabs to the progressive collapse resistance under various column removal scenarios was quantified.

2. Validation of numerical analysis model

2.1. Test specimens for analysis verification

To verify the validity of the FE numerical model, the existing test data conducted by Feng et al. [14] was considered. A total of four half scaled assembled monolithic concrete sub-frame specimens were tested under quasi-static loading. As shown in Fig. 1, two prefabricated beams, two prefabricated exterior columns, and one prefabricated mid-column were assembled in the sub-frame

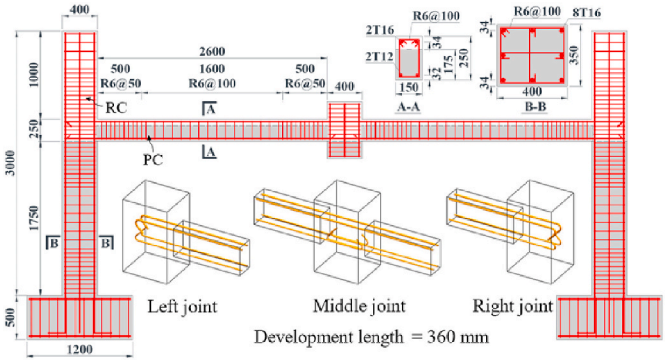

Fig. 1. Reinforcement details of specimen PCF-1.

specimen. Fig. 2 shows the test setup. Pin and fixed boundary conditions were used at the top and bottom of exterior columns, respectively. Guide rail was installed at the front and back sides of the mid-column to address the in-plane and out-of-plane constraints due to the slab and top column. The load was applied by monotonically increasing the vertical displacement of the mid-column until the complete failure of the specimen.

Table 1 shows the reinforcement and joint details of four specimens. The test parameters include the beam dimensions, beam rebar ratio, development length of 135° hooked bars, and connection detail. More detailed information for the experimental program can be found in the literature [14].

2.2. Finite element modeling

In order to fully understand the load transfer mechanism of frame structures under collapse, numerical investigation was performed using commercial software LS-DYNA. The explicit FE method was adopted to avoid the convergence difficulties of traditional implicit FE method at large deformation stage [25,40,41,43].

2.2.1. Element type

In the establishment of the FE model, elements are crucial for the accuracy and reliability of the entire FE analysis. Fig. 3 shows the numerical analysis model of specimen PCF-1. Concrete was modeled using eight-node hexahedral solid elements with reduced integration. Reinforcing bars were modeled using 2-node Hughes-Liu beam elements with 2 × 2 Gauss quadrature integration. The beam element can effectively simulate the mechanical behaviors of rebars, such as axial forces, bi-axial bending, and transverse shear. The loading steel plate and the top constraint device of the exterior column were modeled using eight-node hexahedral solid elements, and the boundary spring was modeled using one-dimensional discrete spring elements. Based on the mesh sensitivity analysis, the mesh size was (12.5–25.0) mm for the beams, and (12.5–50.0) mm for the columns and footings. The smaller mesh size of 12.5 mm was used in the joint region. Note that the cast-in-situ and precast concrete were interconnected via shared nodes since good bonding effect was achieved for four specimens in the tests. Regarding the modeling process of the specimen, the software UG, HyperMesh, and LS-PrePost were adopted for 3D geometric modeling, mesh division, and pre-processing, respectively.

2.2.2. Bond-slip relationship between rebar and concrete

The structural behavior is significantly affected by the bond behavior between rebars and concrete. Addressing cracks in beam-column joint region due to strain concentration and bar-slip, the keyword *CONTACT_1D was used to consider the local bond-slip of beam longitudinal bars in the joint region and plastic hinge region with the length equal to the half of the beam height [40,41]. For the rebars except the joint and plastic hinge region, perfect bond between the rebar and concrete was assumed, and the beam elements were coupled to the concrete elements using the keyword *CONSTRAINED_ LAGRANGE_IN_SOLID.

In this study, to calibrate the properties of CONTACT_1D, the bond-slip relationship specified in Model Code 2010 [46] was employed. The bond stress τ_b between the rebar and concrete can be defined as follows:

$$\tau_b = \begin{cases} \tau_{b\,\max}(s/s_1)^{\alpha} & \text{for} \quad 0 \le s \le s_1 \\ \tau_{b\,\max} & \text{for} \quad s_1 \le s \le s_2 \\ \tau_{b\,\max} - \dfrac{(\tau_{b\,\max} - \tau_{bf})(s - s_2)}{(s_3 - s_2)} & \text{for} \quad s_2 \le s \le s_3 \\ \tau_{bf} & \text{for} \quad s \ge s_3 \end{cases} \tag{1}$$

where the parameters τ_{bmax}, τ_{bf}, s_1, s_2, and s_3 are defined addressing the compressive strength of concrete and the bond conditions [46].

In LS-DYNA, to consider the bond strength degradation after the peak bond stress, an exponential damage curve was used for the bond stress-slip (τ-*s*) relationship of CONTACT_1D [40,41].

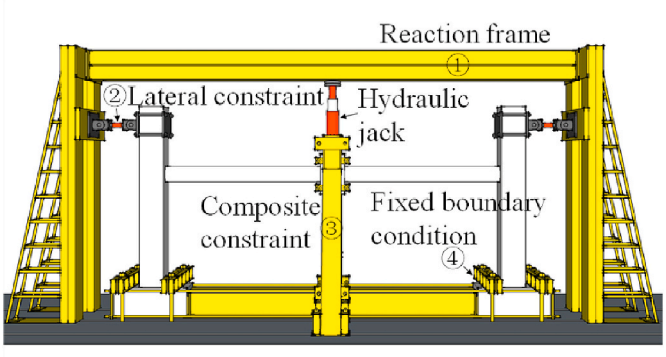

Fig. 2. Test setup.

Table 1
Reinforcement and joint details of specimens [14].

Specimen	Beam					Interior joint		Exterior joint	
	Cross section ($b \times h$) (mm)	Clear span (L_n) (m m)	Flexural bars		Transverse bars	Anchorage method	Hook length (Weld length) (mm)	Anchorage method	Hook length (mm)
			Top	Bottom					
PCF-1	150 × 250	2600	2T16 (1.24 %)	2T12 (0.69 %)	R6@100 (50)	135°hook	360	135°hook	360
PCF-2	180 × 300	2600	4T10 (0.65 %)	1T10+2T8 (0.37 %)	R6@100 (50)	135°hook	360	135°hook	360
PCF-3	180 × 300	2600	4T10 (0.65 %)	1T10+2T8 (0.37 %)	R6@100 (50)	135°hook	195	135°hook	195
PCF-4	150 × 250	2600	2T16 (1.24 %)	2T12 (0.69 %)	R6@100 (50)	Welding	120	135°hook	360

Note: T16 indicates the deformed bar with 16 mm diameter, and R6 indicates the plain bar with 6 mm diameter. The net cover concrete thickness of beam and column sections is 20 mm. The spacing of stirrups in beams and columns is 100 mm. At the beam end and column end, the stirrup spacing is 50 mm.
HRB400 deformed bars were used for flexural bars, and HPB300 plain R6 bars were used for transverse bars. The compressive cylinder strengths of concrete was $f_c' =$ (31.6, 30.0, 32.1 and 32.1) MPa for precast concrete, and $f_c' =$ (26.9, 27.2, 28.3 and 28.3) MPa for cast-in-place concrete.

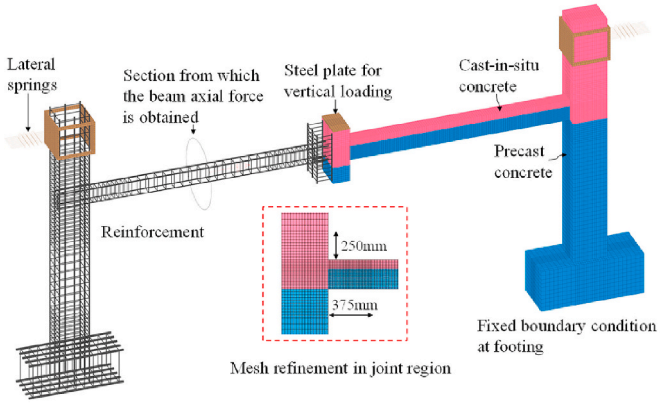

Fig. 3. Numerical analysis model of specimen PCF-1.

$$\tau = \begin{cases} G_b s & \text{for } s \le s_{\max} \\ \tau_{\max} e^{-h_{dmg} D} & \text{for } s > s_{\max} \end{cases} \quad (2)$$

where G_b is the bond shear modulus (=27.4 MPa/mm in this study); $s_{\max}$ is the maximum elastic slip (=0.5 mm in this study); h_{dmg} is the damage curve exponential coefficient (=0.1 in this study); and D ($=s\text{-}s_{\max}$) is the damage parameter. It is noted that the parameter values of the simplified bond-slip model for CONTACT_1D were determined by comparing Eq. (1) and **(2)** [40].

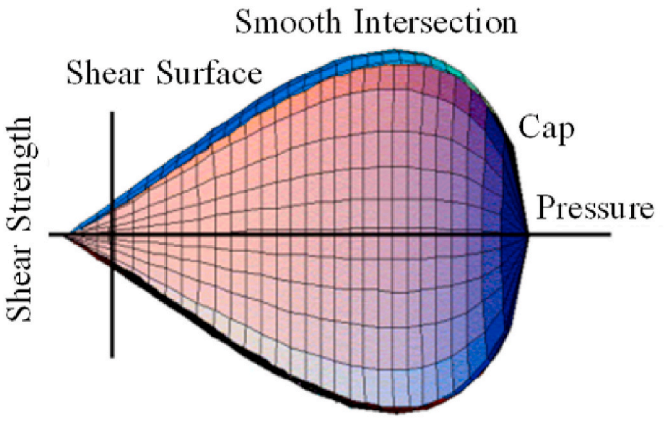

Fig. 4. Yield surface of CSCM.

2.2.3. Material modeling

LS-DYNA provides a wealth of constitutive models for concrete material. Existing studies have shown that the continuous surface cap model (CSCM) can achieve satisfactory analysis results in terms of simulating the quasi-static response of RC structures under the mid-column removal scenario. Fig. 4 shows the yield surface shape of CSCM, which can effectively characterize the material properties of concrete under low confinement situation and tensile stress, such as damage-based softening and modulus reduction, shear dilation, shear compaction, confinement effect, and strain rate effect.

To set CSCM parameters, LS-DYNA provides the original version (*Mat_CSCM) and simplified version (*Mat_CSCM_CONCRETE). For the original version, a total of 37 input parameters are required to define concrete material properties. On the other hand, the simplified version requires only the unconfined concrete compressive strength f_c, the maximum aggregate size A_g, and the units. The other relevant parameters can be automatically generated by CSCM itself. According to Yu et al. [41], the use of the default CSCM parameters in the simplified version overestimates the stiffness and load-carrying capacity of the test specimens. To solve such overestimation, the tensile fracture energy G_{ft} can be reduced to 80 % of the default value [47]. In the case of obvious compression or shear damage, the reduced compressive fracture energy $G_{fc} = 50\ G_{ft}$ (default value of $G_{fc} = 100\ G_{ft}$) or reduced shear fracture energy $G_{fs} = 0.5\ G_{ft}$ (default value of $G_{fs} = G_{ft}$) can be used [47]. Addressing the severe compressive failure of concrete and diagonal shear cracks occurred at the beam ends in the test specimens [14], the original version of CSCM was adopted and the relevant fracture energies were decreased in this study. In the original version of CSCM, the unconfined concrete compressive strength f_c and the maximum aggregate size A_g were defined according to the measured values, and the other parameters are calculated according to the user manual of CSCM [47]. Fig. 5 shows the model parameters of CSCM for precast concrete in specimen PCF-1.

When severe cracking and failure of concrete occur, the maximum principal strain ε_{max} is a suitable criterion for erosion algorithm [25,40,41,43]. According to this method, when the maximum principal strain exceeds the failure principal strain, the corresponding concrete element would be removed. According to Pham and Tan [40], when the failure principal strain is too small, the concrete in the compression zone at the beam end unexpectedly suffers from erosion at large deformation stage. Thus, addressing the large displacement of the mid-column in test specimens, the value of failure principal strain was finally set to 0.25 after multiple trial-and-error calculations in terms of concrete cracking and spalling in tension.

Symmetric bilinear elastic-plastic material model *MAT_PLASTIC_KINEMATIC was selected for rebars. The elastic modulus, yield strength, tangential modulus, and ultimate strain of the material model were determined from the material test results [14]. The loading steel plate at the mid-column and the top constraint device at exterior columns adopted a linear elastic material model *MAT_ELASTIC and a rigid material model *MAT_RIGID, respectively. The density, elastic modulus, and Poisson's ratio of the two materials were determined from the steel parameters. The boundary spring at the top of the exterior columns adopted a linear elastic spring material model *MAT_SPRING_ELASTIC, and the spring stiffness was taken as 10 kN/mm according to the test results [14].

2.2.4. Boundary conditions and loading method

As seen in Fig. 2, the fixed boundary condition at the footing was achieved by restricting the translation in three directions of the bottom nodes, the horizontal translation of the side nodes, and the vertical translation of the top nodes at the footing. Horizontal springs were used to simulate the lateral constraints at the top of the exterior columns (Fig. 3). At the contact surface between the top constraint device and exterior columns, the keyword *Contact_Automatic_Surface_To_Surface was used with both the static and dynamic coefficients of friction setting to 0.2. For the composite constraint, it was achieved by retaining only the vertical displacement of the nodes on the front and back sides of the mid-column.

Vertical loading was implemented by applying the vertical displacement to the steel plate on the mid-column through the keyword

1	MID	RO	NPLOT	INCRE	IRATE	ERODE	RECOV	ITRETRC
	1	0.0024000	1	0.0	0	1.2500000	0.0	0
2	PRED							
	0.0							
3	G	K	ALPHA	THETA	LAMDA	BETA	NH	CH
	1.166e+04	1.277e+04	14.725400	0.3016000	10.500000	0.0192900	0.0	0.0
4	ALPHA1	THETA1	LAMDA1	BETA1	ALPHA2	THETA2	LAMDA2	BETA2
	0.7473500	0.0010700	0.1700000	0.0689600	0.6600000	0.0013360	0.1600000	0.0699600
5	R	XD	W	D1	D2			
	5.0000000	91.300003	0.0500000	2.500e-04	3.492e-07			
6	B	FC	D	GFT	GFS	PWRC	PWRT	PMOD
	100.000000	3.0748000	0.1000000	0.0615000	0.0307500	5.0000000	1.0000000	0.0
7	ETA0C	NC	ETAOT	NT	OVERC	OVERT	SRATE	REP0W
	0.0	0.0	0.0	0.0	0.0	0.0	0.0	0.0

Fig. 5. Model parameters of CSCM for precast concrete of PCF-1 (Units: N, mm, and ms).

*BOUNDARY_PRESCRIBED_MOTION_SET. To avoid severe vibration of structural resistance, the loading speed increased slowly with a small constant acceleration of 0.005 mm/ms^2 at the beginning, and remained constant after the loading time reached 100 ms. The total loading displacement was set to 800 mm, and the loading time was 1650 ms.

2.3. Comparison between the analysis and test results

Fig. 6 compares the predictions with the test results in terms of the vertical load-displacement curves of four specimens. Except for specimen PCF-2 showing early rebar fracture, the load displacement curves of the other three specimens are in good agreement with the test results. The basic characteristics of the curve, such as the ascending section (corresponding to CAA), softening section (i.e., strength degradation) as well as the subsequent ascending section (corresponding to CTA), are well reproduced. As seen in Table 2, except for the slight overestimation of P_{CAA} in PCF-4, the error between the predictions and test results was less than 10%. Due to human error during the assembly of precast concrete beams in specimen PCF-2, the beam bottom bars experienced initial plastic deformation, which decreased the peak strength and did not develop CTA. The discussion of specific reasons can be found in the literature [14].

Because CSCM cannot trace the concrete cracks directly, the effective plastic strain is usually adopted to equivalently represent the damage degree of concrete [41]. In general, the larger effective plastic strain represents the wider crack. Fig. 7 compares the crack pattern and failure modes of the specimens. The FE models simulated well the crack distribution, spalling of concrete, and rebar fracture in specimens at the end of test.

In summary, the load displacement curves, crack patterns, and failure modes simulated by the FE method were in good agreement with the test results. The validity and reliability of the FE model were verified. On this basis, the verified FE model was extended to investigate the effects of multi-span continuous beams, simplified boundary conditions, and various column removal scenarios on the progressive collapse resistance of moment frames.

3. Effects of multi-span continuous beams and simplified boundary conditions

Due to the limitations of laboratory space, specimen size, and equipment, most of the existing experimental studies have focused on double-span beam-column substructures. To consider the potential influence of continuous span beams, test specimens are usually simplified assuming a fixed end constraint at the end of the substructure [7–9], a horizontal constraint on the beam extension section of the substructure [25,49], or conservatively free boundary conditions (i.e., ignoring the influence of continuous span beams) [13,14]. As the effect of multi-span continuous beams on the progressive collapse resistance of substructures and the rationality of the simplified boundary conditions have not been completely and explicitly investigated, the effects of multi-span continuous beams and simplified constraint conditions on the progressive collapse resistance of the substructures needs to be evaluated.

3.1. Evaluation of multi-span continuous beam effect

In the validated FE model of specimen PCF-1, one and two spans were additionally attached on the left side in PCF-L1 and PCF-L2, respectively, to consider the effect of multi-span continuous beams on the progressive collapse resistance of the substructure under the penultimate column removal scenario. Further, addressing the column failure at the middle region of moment frames, based on PCF-L2, a new span and two new spans were added to the right side in PCF-L2R1 and PCF-L2R2, respectively. Fig. 8 shows the failure modes

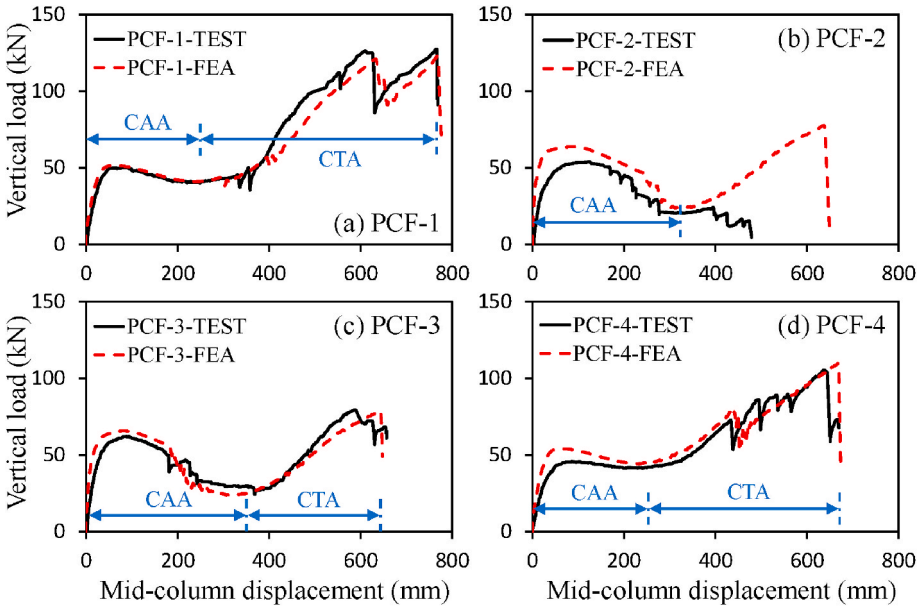

Fig. 6. Comparison of load-displacement curves between analysis and test results.

Table 2
Comparison of key results between numerical analysis and test.

Specimen	P_{CAA} (kN)			E_{CAA} (kJ)			P_{CTA} (kN)			E_{CTA} (kJ)			δ_{CTA} (mm)		
	Test	FE	Rat.	Test	FE	Rat.	Test	FE	Rat.	Test	FE	Rat.	Test	FE	Rat.
PCF-1	50.5	51.6	1.02	10.7	11.2	1.05	127.4	122.7	0.96	55.9	54.3	0.97	765.5	767.7	1.00
PCF-2	54.0	63.8	1.18	12.7	16.3	1.28	N/A	77.6	N/A	N/A	32.1	N/A	N/A	637.4	N/A
PCF-3	62.5	65.7	1.05	15.5	16.0	1.03	79.3	79.1	1.00	32.0	31.3	0.98	586.0	641.9	1.10
PCF-4	45.8	54.0	1.18	10.1	11.8	1.17	105.4	109.7	1.04	39.5	42.8	1.08	636.7	669.3	1.05

Note: E_{CAA} and E_{CTA} are the energy dissipations during the CAA stage and the whole loading process, respectively [48].

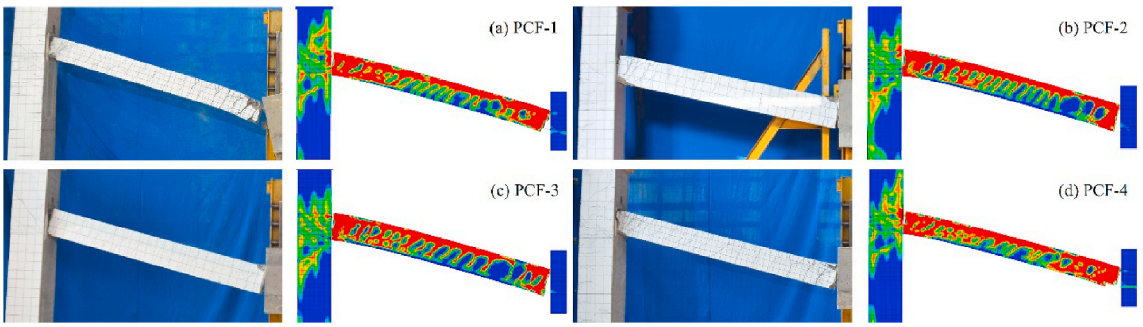

Fig. 7. Comparison of crack patterns and failure modes of specimens at the end of test.

of the four models. Due to the existence of the left side spans, the damage of left exterior column of PCF-L1 and PCF-L2 was significantly less than that of the right exterior column (Fig. 8(a) and (b)). For PCF-L2R1 and PCF-L2R2, compared to PCF-L2, the existence of the right side spans reduced the damage of the right exterior column (Fig. 8(c) and (d)).

Fig. 9(a) compares the vertical load-displacement relationships of the models PCF-1, PCF-L1, and PCF-L2. When a single span was added to the left side, the peak strength at CAA increased from 51.6 kN to 62.4 kN (i.e., an increase of 20.9 %). The additional span increased the lateral stiffness of the left side, which increased the axial compressive force on the beam section (refer to Fig. 9(b)), thereby improving the CAA strength. When another span was further added to the left, the continuous span beam effect was negligible, showing only the axial compressive force increased by 2.0 % in PCF-L2. At CTA stage, the existence of continuous span beams resulted in early development of CTA. However, the effect of continuous span beams on the CTA strength was insignificant due to the sufficient strength of the original exterior columns of the substructure. As seen in Fig. 9(c), when a new span was further added on the right, the peak strength at CAA of PCF-L2R1 was 6.2 % greater than that of PCF-L2 due to the increased beam axial compressive force. However, when another span was additionally added to the right, the side span effect was negligible. Also, the effect of side span on the CTA strength was insignificant due to the sufficient strength of the original exterior columns of the substructure. It is noted that exterior column's strength and stiffness would be relatively weak in real structures in some cases. In this case, the possible effect of exterior

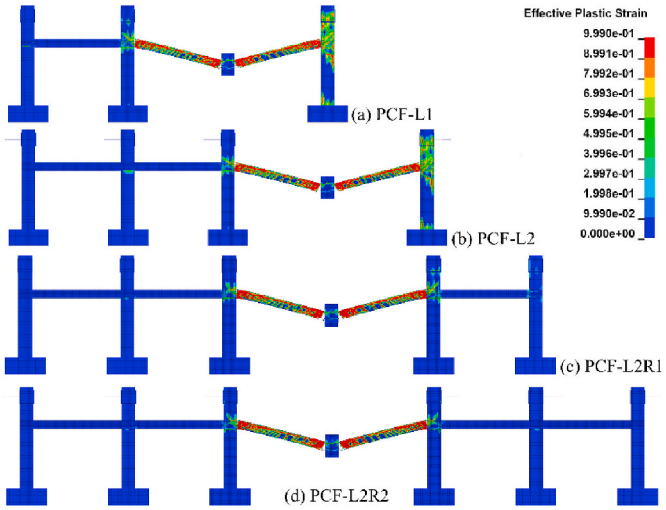

Fig. 8. Failure modes of four models with continuous span beams.

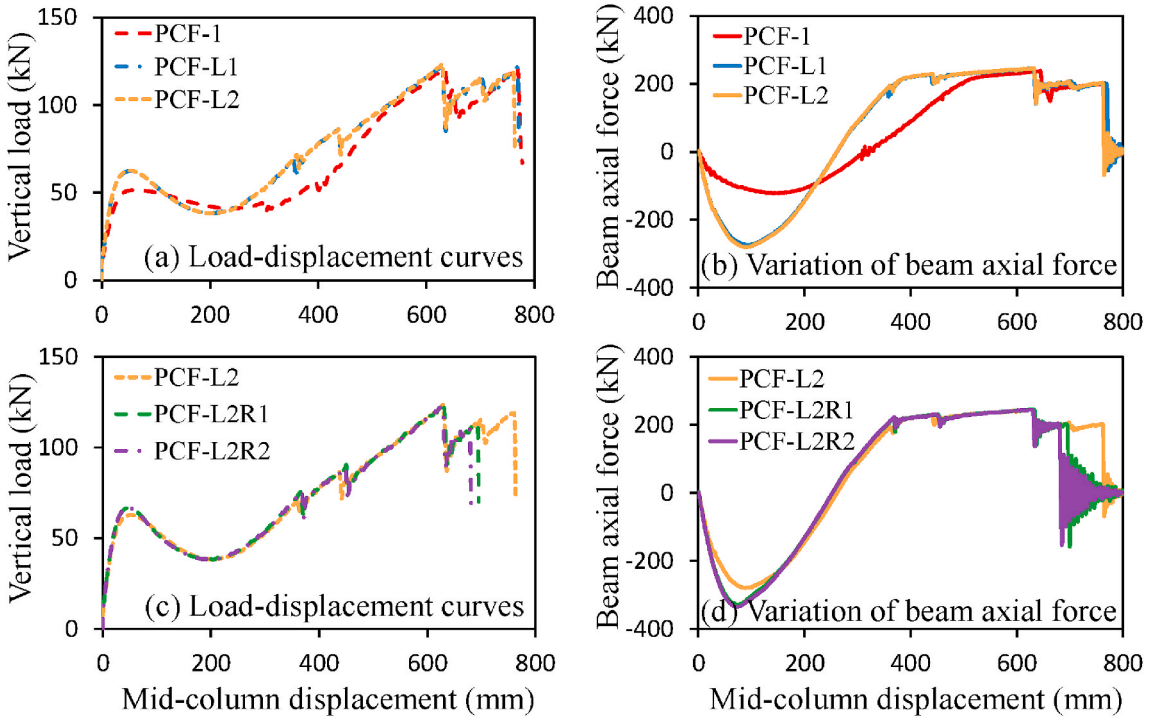

Fig. 9. Analysis results of four models with continuous span beams.

column's strength and stiffness on the progressive collapse resistance of the substructure needs to be systematically evaluated.

3.2. *Evaluation of simplified boundary conditions*

For simple analysis modeling and test setup, a reasonable simplification of boundary conditions is necessary. To describe the continuous span beams, three different beam end constraints (i.e., horizontal constraint, roller support, and fixed boundary condition) were considered in analysis models PCF-1-H, PCF1–V, and PCF-1-F, respectively (Fig. 10).

Fig. 11 shows the failure modes of three FE models. Addressing symmetry condition, only the left half is expressed. Compared with the failure mode of PCF-L2R2 (Fig. 8(d)), the damage of exterior column of PCF-1-H and PCF-1-V was relatively larger due to the simplified boundary constraints. However, due to the full constraint applied to the beam end, the damage of exterior column of PCF-1-F was significantly lower than that of PCF-1-H and PCF-1-V, which is quite close to that of PCF-L2R2. Fig. 12 compares the vertical load-displacement curves and beam axial force variations in PCF-L2R2, PCF-1-H, PCF-1-V, and PCF-1-F. As shown in Fig. 12(a), the peak strength at CAA of PCF-1-H, PCF-1-V, and PCF-1-F was (64.5, 60.7, and 69.4) kN, respectively. Compared with PCF-1-L2R2 (i.e., 67.0 kN), PCF-1-F overestimated the peak strength at CAA, while PCF-1-V largely underestimated the peak strength at CAA. In PCF-1-H, the peak strength at CAA was only 3.7 % lower than that of PCF-L2R2. Similar to the load displacement curve, the beam axial force variations also presented a similar tendency (Fig. 12(b)). In CTA stage, due to the sufficient strength of exterior columns, the effect of

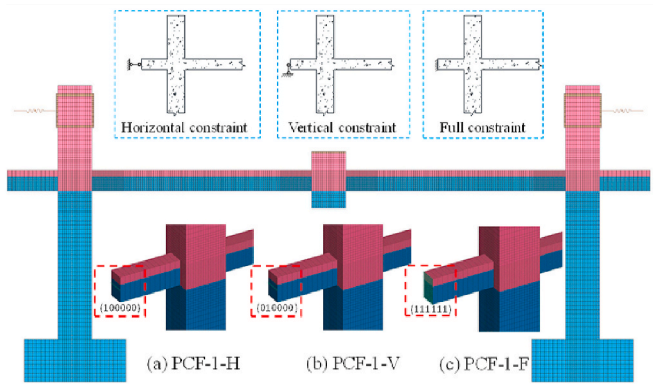

Fig. 10. Numerical analysis models with three simplified boundary conditions.

boundary conditions on the peak strength was insignificant, except for the ultimate displacement corresponding to rebar fracture in PCF-1-V with the reduced lateral stiffness. For simple and conservative analysis modeling, continuous span beams can be replaced with the horizontal constraints. This result is also consistent with the existing research findings that the horizontal constraints applied at the overhang edge of the flat slab substructure are most realistic [43].

4. Effects of transverse beam and slab under penultimate column removal scenario

Although transverse beams and slab can improve the progressive collapse resistance of moment frames, these effects have not been sufficiently evaluated due to the difficulty of tests. For this reason, the contributions of transverse beams and slab to the progressive collapse resistance are not accurately considered in the anti-collapse design of building structures. To consider the bi-directional action, symmetric section was used for the exterior columns (i.e., section dimensions increased from (400 × 350) mm to (400 × 400) mm). For direct comparison, the modified exterior column section was also used in the subsequent 2D analysis model. Further, addressing the convenient modeling and marginal difference between cast-in-situ and assembled monolithic structures, the FEA model was simplified as the cast-in-situ model.

4.1. Evaluation of transverse beam effect

Fig. 13(a) shows the FE model SF-B with a transverse beam. Horizontal constraints were applied to the extension beam ends to approximately consider the influence of continuous span beams in both directions. The design detail of the transverse beam was consistent with that of the longitudinal beam. To accurately evaluate the effect of transverse beam under penultimate column removal scenario, a new model SF-2D was established (Fig. 13(b)). All parameters of the two models are consistent except for the transverse beam.

Fig. 14 shows the failure modes of two models. The failure mode of SF-2D was very similar to the front view of the failure mode of SF-B, and the densely distributed penetrating cracks in the beam indicated the full mobilization of CTA. In the transverse beam of SF-B, flexural cracks were uniformly distributed, and no obvious penetrating cracks occurred. This result indicates that basically no CTA is developed in the transverse beam, which exhibits flexural resistance mechanism during the whole loading process.

Fig. 15(a) compares the vertical load-displacement relationships of SF-B and SF-2D. In small deformation stage (i.e., beam mechanism stage), the use of transverse beam significantly increased the 1st peak strength from 62.3 kN to 84.4 kN (i.e., an increase of 35.5 %). In large deformation stage, although no effective CTA developed in the transverse beam, due to the existence of residual bending strength, the 2nd peak strength of SF-B reached 136.5 kN, which was 13.4 % greater than the 120.4 kN of SF-2D. Fig. 15(b) compares the beam axial force variations of two models. The axial forces on the longitudinal beam section of the two models were basically the same, indicating that the use of the transverse beam hardly affected the CAA and CTA. In the transverse beam, the axial force was negligible, indicating that only the flexural resistance mechanism of the transverse beam should be considered. In practice, when the contribution of a transverse beam to the progressive collapse resistance of moment frames is considered, only the flexural resistance of the transverse beam can be simply included in the vertical load-displacement relationship of the longitudinal subframe.

4.2. Evaluation of slab effect

To quantitatively evaluate the effect of floor slab on the progressive collapse resistance of moment frames, a new model SF-S was established based on the model SF-B. Fig. 16 shows the FE model of SF-S, which consists of two slabs as well as the beams and columns attached to them. Horizontal constraints were applied to the extension segments of the beam and slab to approximately consider the influence of boundary conditions in both directions. Addressing the FE models based on the existing test specimens, the slab was also half scaled. For the concrete and rebars of the slab, the element types and material models were the same as those of the beam. Previous studies have shown that LS-DYNA can accurately simulate the mechanical performance of RC slabs under the column removal scenarios by selecting appropriate element types and material models [21,41,43,50–52].

Fig. 17 shows the failure modes of SF-S. Extensive cracks developed along the top and bottom surface of the slab. Fig. 18 compares the vertical load-displacement relationships of SF-S and SF-B, and the contributions of beams and slab to the progressive collapse resistance of SF-S. As seen in Fig. 18(a), the use of slab increased the 1st peak strength from 84.4 kN to 144.4 kN (i.e., an increase of 71.1 %) in small deformation stage due to the additional compressive membrane action (CMA) developed in the slab. In large deformation stage, the 2nd peak strength of SF-S reached 150.6 kN due to the additional tensile membrane action (TMA) developed in

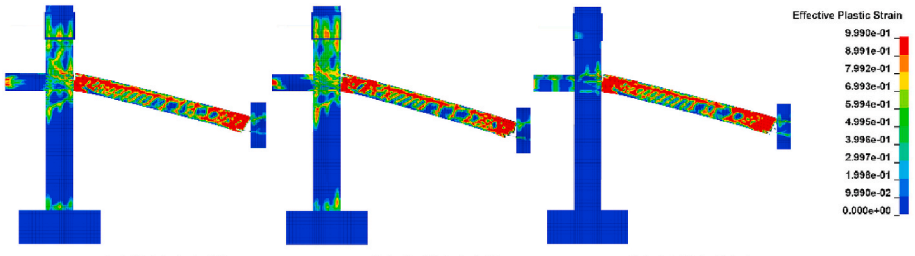

Fig. 11. Failure modes of three models according to boundary conditions.

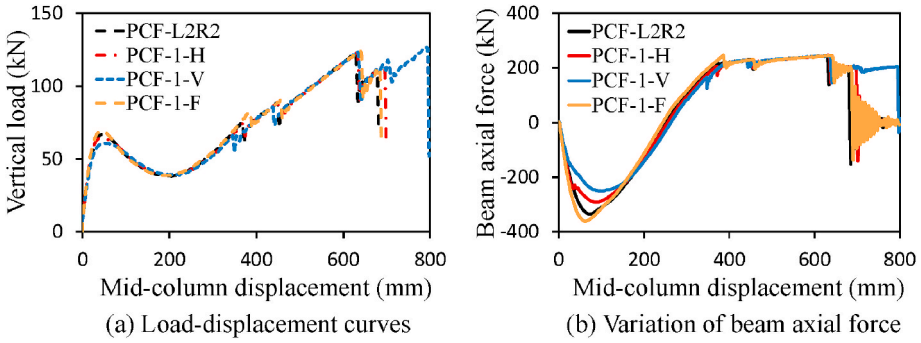

Fig. 12. Analysis results of three models according to boundary conditions.

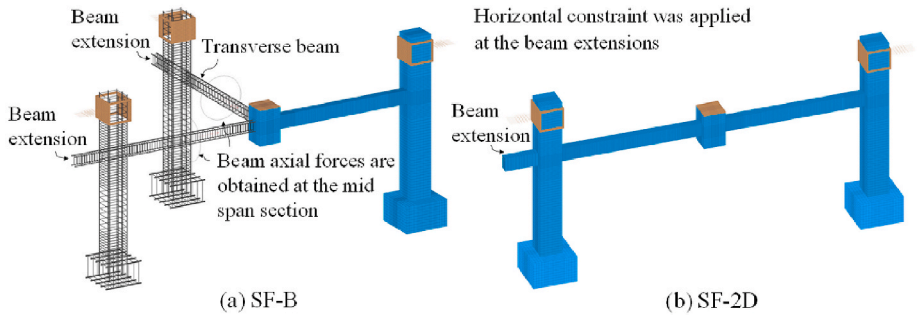

Fig. 13. Numerical analysis models of SF-B and SF-2D.

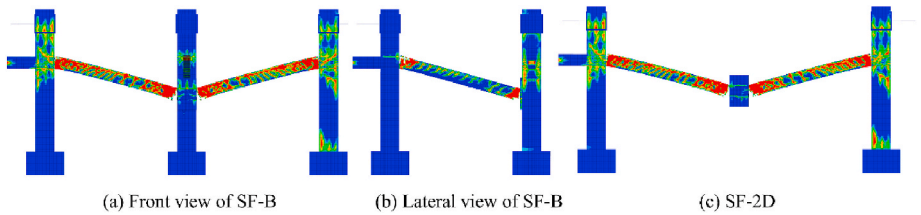

Fig. 14. Failure modes of SF-B and SF-2D.

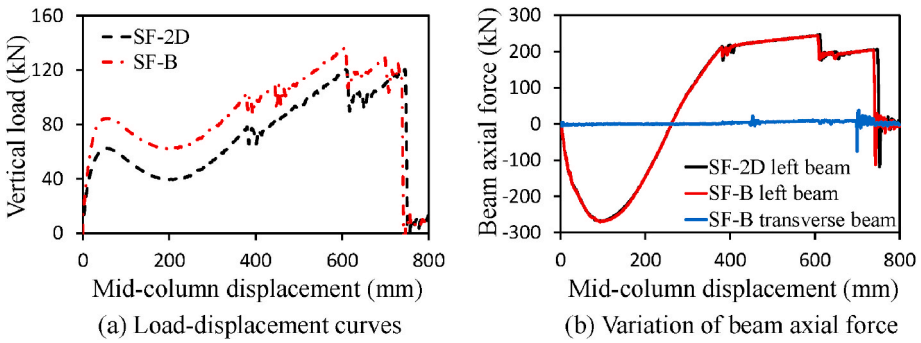

Fig. 15. Analysis results of SF-B and SF-2D.

the slab, which was 89.9 % greater than 79.3 kN of SF-B under the same vertical displacement. After the 2nd peak strength, due to the high restraining effect of slab on the beam deformation, early fracture of the beam bottom bars near the mid-column end occurred, thus leading to the early strength degradation in SF-S. As the mid-column displacement increased, the vertical load gradually increased again due to CTA of beams and TMA of slab, but the resistance of the substructure did not exceed 150.6 kN. When SF-S reached the 1st

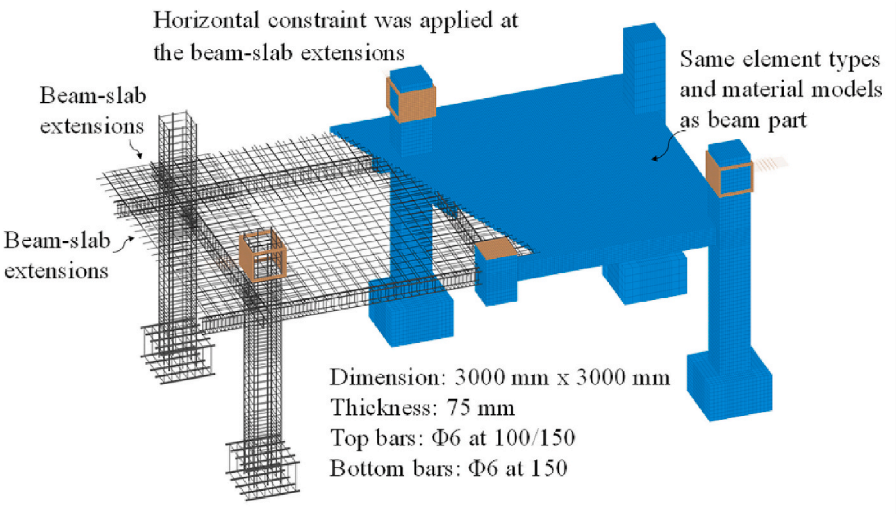

Fig. 16. Numerical analysis model of SF-S

peak strength, the contributions of beams and slab to the load resistance were 58.4 % and 41.6 %, respectively (Fig. 18(b)). As the mid-column displacement increased, the slab contribution gradually increased. When the mid-column displacement reached about 219 mm, the maximum slab contribution was 54.2 %. Ultimately, fracture of beam and slab rebars decreased the slab contribution. Compared to CTA of beams, earlier developed TMA of slabs generates enough secondary resistance mechanism, which improves the progressive collapse resistance. Thus, for economical anti-collapse design in practice, the additional CMA of slab needs to be considered when an exterior column is removed.

5. Effect of column removal scenarios

Location of removed column determines the boundary conditions of substructures and the number of resistant members under collapse, which critically affect the progressive collapse resistance of the substructures. Thus, the effect of column removal scenarios on the progressive collapse resistance of moment frames with/without slabs needs to be quantitatively evaluated.

5.1. Column removal in subframes without slab

Based on the original removal scenario of the penultimate column (scenario 1), the other four column removal scenarios corresponding to scenarios 2 to 5 were investigated (Fig. 19). Fig. 20 shows the failure modes of four models. Regarding the model name, the last number denotes the column removal scenario number. Except the transverse beam in SF-B-2 with a single transverse beam, large number of penetrating cracks were distributed along all longitudinal and transverse beams, indicating the sufficient development of CTA.

Fig. 21 compares the vertical load-displacement relationships of models SF-B-1 to SF-B-5. For direct comparison, the vertical load-displacement relationship of SF-B was also included as SF-B-1 in this figure. Compared to SF-B-1, the 1st and 2nd peak strengths of SF-B-2 increased by (4.5 and 1.9)%, respectively, due to the influence of the right beam end constraint. Due to the CAA developed in transverse beams, the maximum 1st peak strength of SF-B-3, SF-B-4, and SF-B-5 was 133.1 kN, which was 50.9% greater than that of SF-B-1 and SF-B-2. In large deformation stage, due to the CTA developed in transverse beams, the maximum 2nd peak strength of SF-B-3, SF-B-4, and SF-B-5 was 239.2 kN, which was 72.0% greater than that of SF-B-1 and SF-B-2. Regardless of beam end constraint, the progressive collapse resistance can be simply grouped according to the location of removed column (i.e., scenarios 1 to 2 for exterior column removal and scenarios 3 to 5 for interior column removal). Compared to PCF-1-H without transverse beams (Fig. 12(a)), the 1st and 2nd peak strengths of SF-B-5 with transverse beams increased by (106.4 and 87.1)%, respectively. This result indicates that use of double-span transverse beams can linearly increase the peak strengths of CAA and CTA. However, due to the different mid-column displacement at rebar fracture, the peak strengths of SF-B-5 would not be exactly twice that of PCF-1-H.

Fig. 22(a) compares the beam axial forces in the longitudinal direction of models SF-B-1 to SF-B-5. At CAA, the beam axial forces of the five models were almost the same. Due to the horizontal constraints at both beam ends, the axial compressive force in the beams of SF-B-2, SF-B-4, and SF-B-5 was increased by 10.6%, compared to SF-B-1 and SF-B-3. At CTA, due to the sufficient strength of the exterior columns, the axial tensile force in the beams of the five models were basically consistent. Fig. 22(b) compares the beam axial forces in the transverse direction. The beam axial force of SF-B-1 and SF-B-2 was negligible. As SF-B-3, SF-B-4, and SF-B-5 also had double-span beams in the transverse direction, the beam axial forces were fully mobilized. Due to the stronger boundary constraints in the transverse direction of SF-B-5, its beam axial force was 7.6% greater than that of SF-B-3 and SF-B-4 at CAA. At CTA, the axial tensile force of the beams in the three models were basically the same.

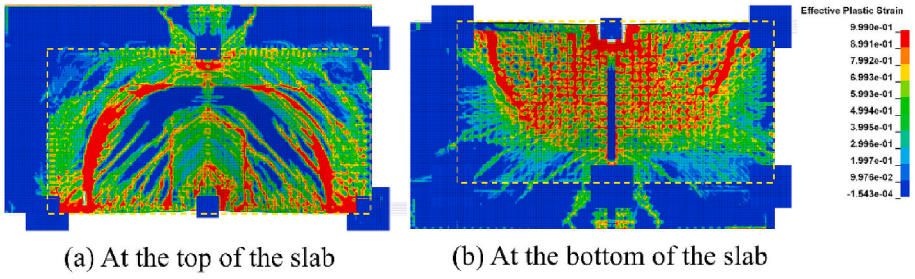

Fig. 17. Failure modes of SF-S

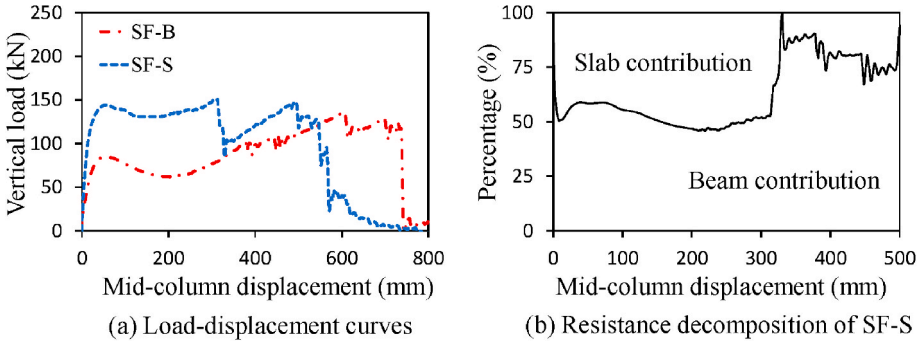

Fig. 18. Comparisons between SF-S and SF-B

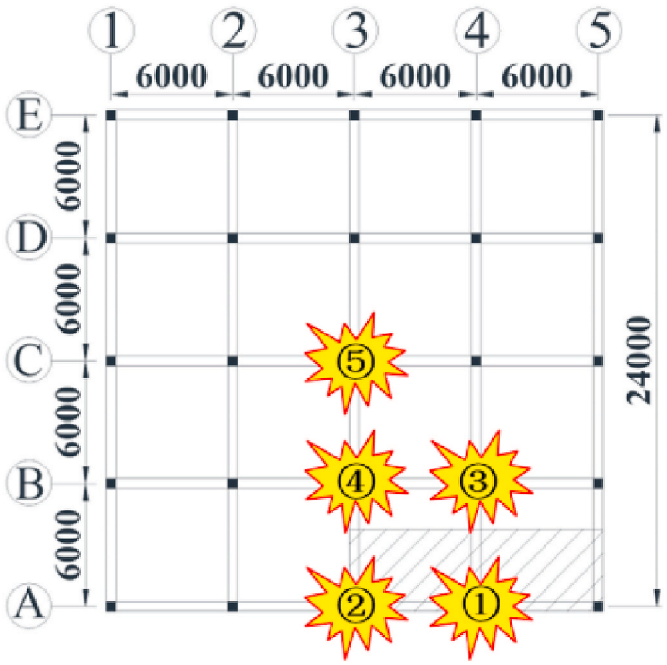

Fig. 19. Possible column removal scenarios in moment frames.

5.2. Column removal in subframes with slab

To quantitatively evaluate the effect of slab on the progressive collapse resistance of the substructure under different column removal scenarios, based on the original removal scenario of the penultimate column (scenario 1), the other four column removal scenarios corresponding to scenarios 2 to 5 were investigated (Fig. 23). As in the previous section, horizontal constraints are applied to the extension segments of the beams and slabs to approximately consider the influence of boundary conditions in both directions.

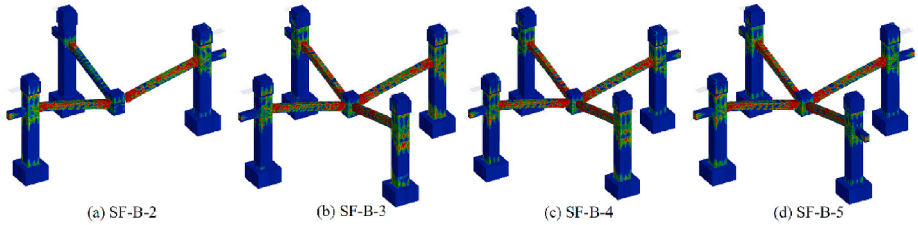

Fig. 20. Failure modes of models according to column removal scenarios.

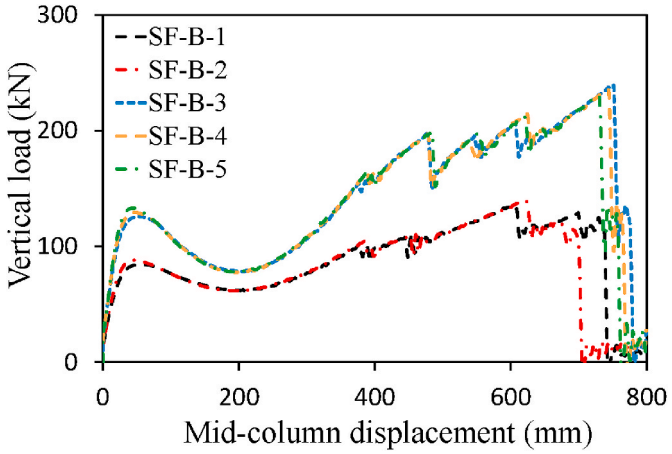

Fig. 21. Comparison of load-displacement curves of models according to column removal scenarios.

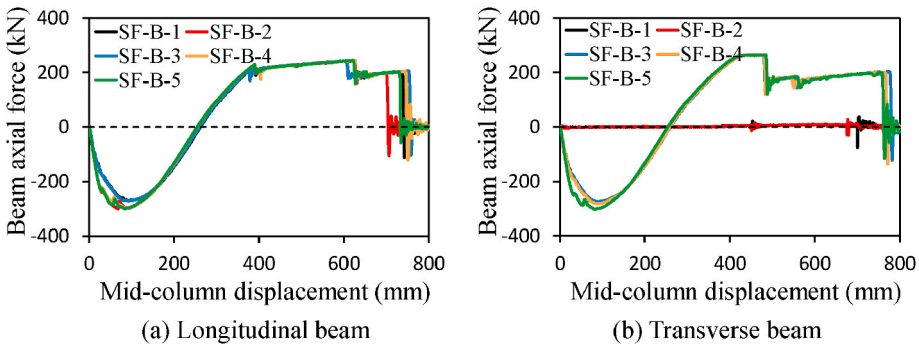

Fig. 22. Comparison of beam axial forces of models according to column removal scenarios.

Fig. 24 shows the failure modes of SF-S-5. Compared to SF-S (Fig. 17), the crack patterns of SF-S-5 presented a symmetric distribution in both directions, and the CMA and TMA of the substructure were fully mobilized. Fig. 25 compares the vertical load-displacement curves of models SF-S-1 to SF-S-5. For direct comparison, the prediction of SF-S was also included as SF-S-1 in this figure. During the small deformation stage, the peak strength of SF-S-2 was 5.6% greater than that of SF-S-1 due to the horizontal

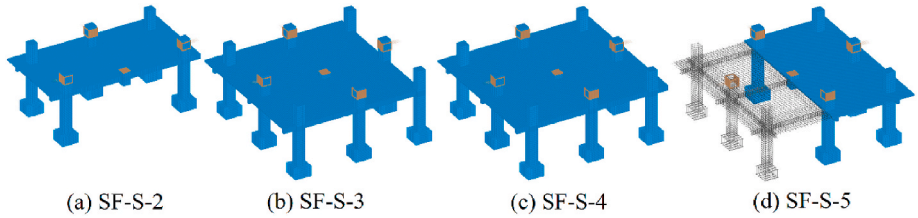

Fig. 23. Numerical analysis models with slab.

constraint on the right beam-slab extension section of SF-S-2. When double-span beams were used in the transverse direction, the maximum 1st peak strength of SF-S-3, SF-S-4, and SF-S-5 was 247.3 kN, which was 62.2% greater than that of SF-S-1 and SF-S-2. In large deformation stage, due to TMA fully developed in the slab, the maximum 2nd peak strength of SF-S-3, SF-S-4, and SF-S-5 was 349.8 kN, which was 132.3% higher than that of SF-S-1 and SF-S-2. Compared to SF-S-1 and SF-S-2, strength degradation was insignificant in SF-S-3, SF-S-4, and SF-S-5, and a continuous increase in strength was achieved due to the full mobilization of TMA. Further, as seen in Figs. 24 and 25, unlike the CMA of slab, the TMA does not require high constraints on the edge of the slab, since the existence of the compression ring around the slab itself can provide sufficient lateral constraints for the TMA developed in the middle region.

Besides, compared with the subframes without slab (Fig. 21), the additional CMA of slab improved the progressive collapse resistance of the moment frames by 71–73%, for the exterior column removal scenarios. For the interior column removal scenarios, the additional CMA and TMA of slab further improved the progressive collapse resistance of the moment frames by 86% and 46%, respectively.

Comparing the resistance curves of SF-S series and SF-B series, the load contribution ratio of beams and slabs in the substructure can be quantified (Fig. 26). When the substructures reached the 1st peak strength, the slab of SF-S-2, SF-S-3, SF-S-4, and SF-S-5 resisted (42.0, 43.3, 44.6, and 45.9)% of the vertical load, respectively. The slab contribution to the collapse resistance in the four models was similar. As the mid-column displacement increased, the slab contribution gradually increased, especially in SF-S-3, SF-S-4, and SF-S-5. The slab contribution of SF-S-3, SF-S-4, and SF-S-5 was significantly greater than that of SF-S-2 with a single transverse beam. The maximum slab contribution ratio of the four models reached (54.8, 74.1, 74.8, and 75.1)%, respectively. In the large displacement stage, due to the full mobilization of the TMA within the slab of SF-S-3, SF-S-4, and SF-S-5, the slab contribution ratio of the three models was significantly higher than that of SF-S-2.

6. Discussion of dynamic effects

The simplified energy balance method proposed by Izzuddin et al. [48] provides an effective approach for evaluating the dynamic collapse resistance of structures. In this method, the pseudo-static resistance of the structure is determined from the external work ($P_d \cdot \delta_p$) produced by dynamic load and the strain energy ($\int_0^{\delta_p} P(\delta)d\delta$) absorbed by the structure (refer to Fig. 27(c)).

$$P_d \cdot \delta_p = \int_0^{\delta_p} P(\delta)d\delta \tag{3}$$

where P_d is dynamic load; δ_p is the predicted displacement corresponding to P_d; and $P(\delta)$ is the vertical load measured from the static loading test or static analysis.

Fig. 27 compares the pseudo-static resistance of SF-S-2, SF-S-3, SF-S-4, and SF-S-5. The peak pseudo-static resistances of the four models are (135.7, 278.8, 283.9, and 285.8) kN, respectively. Through this method, it is possible to directly estimate the allowable anti-collapse design load or the displacement corresponding to the collapse resistance under design load (refer to Fig. 27(d)), without complicated nonlinear dynamic analysis. However, it has been pointed out that the displacement predicted by the simplified energy balance method is usually larger than the actual value, since it ignores the effects of damping and strain rate on the material strength [14,53]. For this reason, this method can be conveniently used for conservative design at initial design step. To verify the usefulness of the simplified energy balance method in various design conditions, further study is needed to compare the nonlinear dynamic analysis results in the FE modeling method validated in this study.

7. Summary and conclusions

In this study, the progressive collapse performance of frame structures was systematically analyzed using LS-DYNA software. After careful calibration of model parameters, the numerical models were validated through comparisons with experimental results and further employed to investigate the effects of multi-span continuous beams, simplified boundary conditions, and various column removal scenarios on the progressive collapse resistance. The primary findings can be summarized as follows.

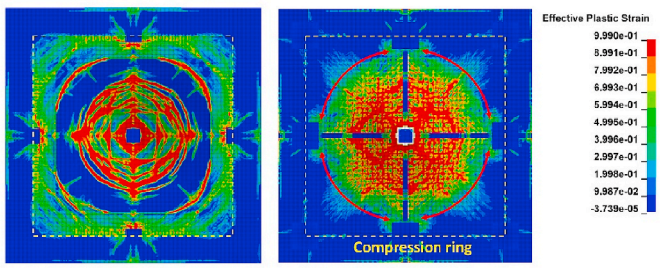

(a) At the top of the slab (b) At the bottom of the slab

Fig. 24. Failure modes of SF-S-5.

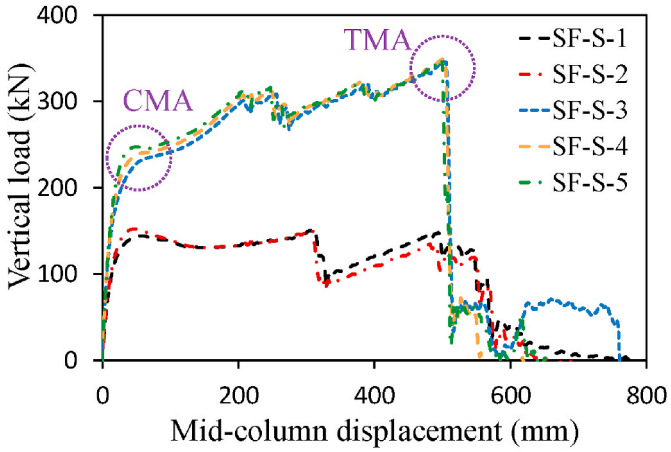

Fig. 25. Comparison of load-displacement curves of models with slab according to column removal scenarios.

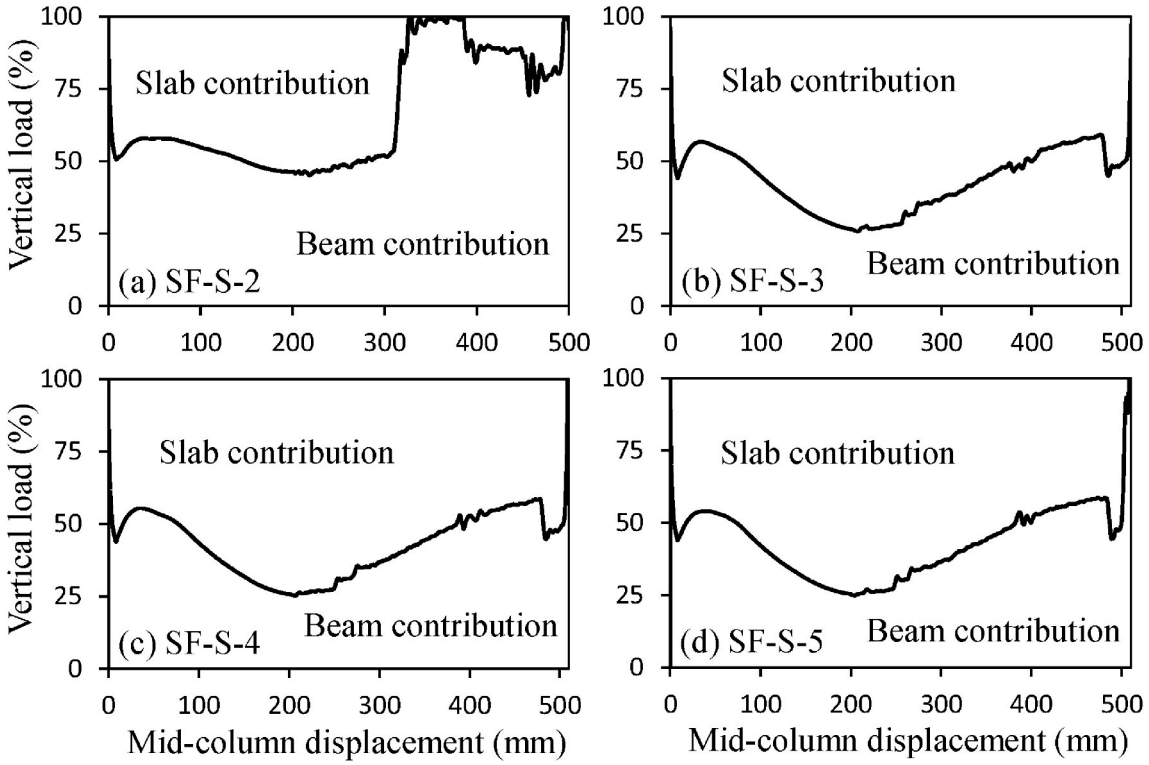

Fig. 26. Quantification of collapse resistance of the slab in models SF-S-2~SF-S-5.

1. To predict the progressive collapse resistance of frame structures under static loading, a refined numerical model was considered. The load displacement curves, crack patterns, and failure modes of the FE analysis results were in good agreement with the experimental results.
2. Compared with the subframe without continuous span beams, use of continuous span beam increased the peak strength at CAA. However, the strength increase was not linearly affected by the additional continuous span beams at both sides. In moment frames satisfying strong column-weak beam concept, use of continuous span beam did not increase the peak strength at CTA, but resulted in early development of CTA.
3. To represent the effect of continuous span beams reasonably, three different simplified boundary conditions were compared, namely, horizontal constraints, vertical constraints, and full constraints. The results showed that for simple analysis modeling, continuous span beams can be replaced with the horizontal constraints at the extended beams.

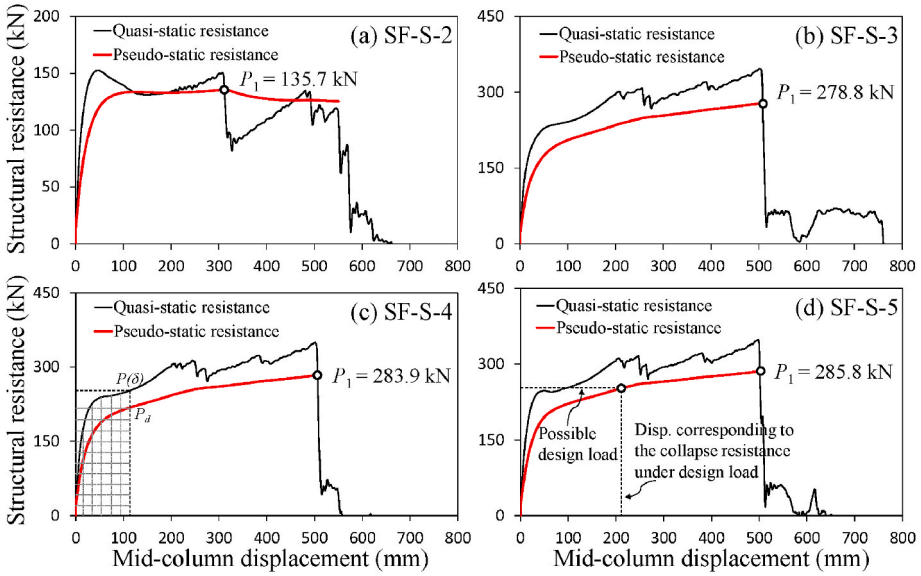

Fig. 27. Pseudo-static resistance of SF-S-2~SF-S-5.

4. When the contribution of a transverse beam to the progressive collapse resistance of moment frames is considered (i.e., removal of an exterior column), the flexural resistance of the transverse beam can be simply included in the progressive collapse resistance of the subframe without transverse beams. The additional CMA of slab improved the progressive collapse resistance of the moment frames by 71–73 % before the development of CTA of beams, which allowed economical anti-collapse design in practice for the exterior column removal scenario.
5. When the contribution of double-span transverse beams to the progressive collapse resistance of moment frames is considered (i.e., removal of an interior column), the peak strengths of CAA and CTA of the transverse beams can be simply included in the progressive collapse resistance of the subframe without transverse beams. The additional CMA and TMA of slab further improved the progressive collapse resistance of the moment frames by 86 % and 46 %, respectively. Thus, the slab contribution needs to be considered for economical anti-collapse design in practice for the interior column removal scenario.

In this study, nonlinear static behavior of moment frames with various collapse conditions was investigated. To accurately evaluate the actual progressive collapse behavior of moment frames, further study on nonlinear dynamic analysis is needed using the validated FE modeling method. Besides, for PC structures with half PC slab and topping concrete, it can show the full or partial composite action between the slab and moment frame according to the connection details. The partial composite action would decrease the strength due to CAA and membrane action, and increase the deformation capacity due to lower restraint. For simplicity, RC slab was adopted in this study. The exact PC slab effect on the overall collapse behavior of the PC structures needs to be further investigated.

CRediT authorship contribution statement

Fei-Fan Feng: Writing – original draft, Methodology, Investigation, Formal analysis, Data curation. **Hyeon-Jong Hwang:** Writing – original draft, Supervision, Project administration, Methodology, Conceptualization. **Yun Zhou:** Writing – review & editing, Validation, Project administration. **Jing-Ming Sun:** Investigation, Formal analysis. **Hu-Zhi Zhang:** Formal analysis. **Jun-Ho Roh:** Formal analysis. **Su-Min Kang:** Validation. **Wei-Jian Yi:** Supervision.

Declaration of competing interest

The authors declare that they have no known competing financial interests or personal relationships that could have appeared to influence the work reported in this paper.

Data availability

Data will be made available on request.

Acknowledgments

This research was financially supported by Korea Agency for Infrastructure Technology Advancement (KAIA) grant funded by the Ministry of Land, Infrastructure and Transport (Grant 22RMPP-C163162-02); and Human Resources Development Program of the Korea Institute of Energy Technology Evaluation and Planning (KETEP) grant funded by the Ministry of Trade, Industry and Energy,

Republic of Korea (No. RS-2023-00237035). The authors are grateful to the authorities for the supports.

References

[1] J.M. Adam, F. Parisi, J. Sagaseta, X.Z. Lu, Research and practice on progressive collapse and robustness of building structures in the 21st century, Eng. Struct. 173 (2018) 122–149.
[2] J.K. Hong, T.H.-K. Kang, Computing in protection engineering: CFD analysis of blade fragment impact on concrete wall, J Struct Integrity Maint 3 (4) (2018) 210–216.
[3] Department of Defence (DoD), Design of Buildings to Resist Progressive Collapse (UFC 4-023-03), Unified Facilities Criteria, Washington, DC, 2013.
[4] General Services Administration (GSA), Alternative Path Analysis and Design Guidelines for Progressive Collapse Resistance, Office of Chief Architects, Washington, DC, 2013.
[5] China Association for Engineering Construction Standardization (CECS), Code for anti-collapse design of building structures, CECS 392 (2014). Beijing (China).
[6] W.J. Yi, F. Yi, Y. Zhou, Experimental studies on progressive collapse behavior of RC frame structures: advances and future needs, Int. J. Concrete Struct. Mater. 15 (2021) 31.
[7] J. Yu, K.H. Tan, Experimental and numerical investigation on progressive collapse resistance of reinforced concrete beam column sub-assemblages, Eng. Struct. 55 (2013) 90–106.
[8] K. Qian, B. Li, Performance of three-dimensional reinforced concrete beam column substructures under loss of a corner column scenario, J. Struct. Eng. 139 (4) (2013) 584–594.
[9] S.B. Kang, K.H. Tan, Behaviour of precast concrete beam column sub-assemblages subject to column removal, Eng. Struct. 93 (2015) 85–96.
[10] B. Yang, K.H. Tan, G. Xiong, S.D. Nie, Experimental study about composite frames under an internal column-removal scenario, J. Constr. Steel Res. 121 (2016) 341–351.
[11] H.S. Lew, J.A. Main, Y. Bao, F. Sadek, V.P. Chiarito, S.D. Robert, et al., Performance of precast concrete moment frames subjected to column removal: part 1, experimental study, PCI J. (Sept–Oct) (2017) 35–52.
[12] Y. Zhou, T.P. Chen, Y.L. Pei, H.J. Hwang, X. Hu, W.J. Yi, L. Deng, Static load test on progressive collapse resistance of fully assembled precast concrete frame structure, Eng. Struct. 200 (2019) 109719.
[13] Y. Zhou, X. Hu, Y.L. Pei, H.J. Hwang, T.P. Chen, W.J. Yi, L. Deng, Dynamic load test on progressive collapse resistance of fully assembled precast concrete frame structures, Eng. Struct. 214 (2020) 110675.
[14] F.F. Feng, H.J. Hwang, W.J. Yi, Static and dynamic loading tests for precast concrete moment frames under progressive collapse, Eng. Struct. 213 (2020) 110612.
[15] Z.D. Zhao, X.W. Cheng, Y. Li, M.Z. Diao, H. Guan, Y. An, Progressive collapse analysis of precast reinforced concrete beam-column assemblies with different dry connections, Eng. Struct. 287 (2023) 116174.
[16] X.D. Pham, K.H. Tan, Experimental response of beam-slab substructures subject to penultimate-external column removal, J. Struct. Eng. 141 (7) (2015) 04014170.
[17] P.Q. Ren, Y. Li, X.Z. Lu, H. Guan, Y.L. Zhou, Experimental investigation of progressive collapse resistance of one-way reinforced concrete beam–slab substructures under a middle-column-removal scenario, Eng. Struct. 118 (2016) 28–40.
[18] N.S. Lim, K.H. Tan, C.K. Lee, Experimental studies of 3D RC substructures under exterior and corner column removal scenarios, Eng. Struct. 150 (2017) 409–427.
[19] X.Z. Lu, K.Q. Lin, Y. Li, H. Guan, P.Q. Ren, Y.L. Zhou, Experimental investigation of RC beam-slab substructures against progressive collapse subjected to an edge-column-removal scenario, Eng. Struct. 149 (2017) 91–103.
[20] K. Qian, B. Li, Investigation into resilience of precast concrete floors against progressive collapse, ACI Struct. J. 116 (2) (2019) 171–182.
[21] J. Yu, J.H. Tang, L.Z. Luo, Q. Fang, Effect of boundary conditions on progressive collapse resistance of RC beam-slab assemblies under edge column removal scenario, Eng. Struct. 225 (2020) 111272.
[22] Y.D. Zhang, X.W. Cheng, M.Z. Diao, Y. Li, H. Guan, H.L. Sun, FRP retrofit for RC frame substructures against progressive collapse: scheme optimisation and resistance calculation, Eng. Struct. 289 (2023) 116289.
[23] W.J. Yi, Q.F. He, Y. Xiao, S.K. Kunnath, Experimental study on progressive collapse-resistant behavior of reinforced concrete frame structures, ACI Struct. J. 105 (4) (2008) 433–439.
[24] N. Khorsandnia, H. Valipour, S. Foster, A. Amin, Experimental study of progressive collapse resistance of reinforced concrete framed structures, ACI Struct. J. 114 (6) (2017) 1385–1396.
[25] K. Qian, Y.H. Weng, B. Li, Improving behavior of reinforced concrete frames to resist progressive collapse through steel bracings, J. Struct. Eng. 145 (2) (2019) 04018248.
[26] S. Shan, S. Li, S. Xu, L. Xie, Experimental study on the progressive collapse performance of RC frames with infill walls, Eng. Struct. 111 (2016) 80–92.
[27] Y. Xiao, S. Kunnath, F.W. Li, Y.B. Zhao, H.S. Lew, Y. Bao, Collapse test of three-storey half-scale reinforced concrete frame building, ACI Struct. J. 112 (4) (2015) 429–438.
[28] M.Z. Diao, Y. Li, H. Guan, X.Z. Lu, B.P. Gilbert, Influence of horizontal restraints on the behaviour of vertical disproportionate collapse of RC moment frames, Eng. Fail. Anal. 109 (2020) 104324.
[29] J.X. Wang, Y.H. Sun, S. Gao, W.D. Wang, Anti-collapse performance of concrete-filled steel tubular composite frame with RC shear walls under middle column removal, J. Build. Eng. 64 (2023) 105611.
[30] K.Q. Lin, X.Z. Lu, Y. Li, H. Guan, Experimental study of a novel multi-hazard resistant prefabricated concrete frame structure, Soil Dynam. Earthq. Eng. 119 (2019) 390–407.
[31] X.Z. Lu, L. Zhang, K.Q. Lin, Y. Li, Improvement to composite frame systems for seismic and progressive collapse resistance, Eng. Struct. 186 (2019) 227–242.
[32] Y. Tian, K.Q. Lin, X.Z. Lu, L. Zhang, Y. Li, H. Guan, Experimental and theoretical study of seismic and progressive collapse resilient composite frames, Soil Dynam. Earthq. Eng. 139 (2020) 106370.
[33] J. Yu, K.H. Tan, Analytical model for the capacity of compressive arch action of re-inforced concrete sub-assemblages, Mag. Concr. Res. 66 (3) (2014) 109–126.
[34] S.B. Kang, K.H. Tan, Analytical model for compressive arch action in horizontally restrained beam-column subassemblages, ACI Struct. J. 113 (4) (2016) 813–826.
[35] X.Z. Lu, K.Q. Lin, C.F. Li, Y. Li, New analytical calculation models for compressive arch action in reinforced concrete structures, Eng. Struct. 168 (2018) 721–735.
[36] P. Stylianidis, D. Nethercot, B. Izzuddin, A. Elghazouli, Study of the mechanics of progressive collapse with simplified beam models, Eng. Struct. 117 (2016) 287–304.
[37] S. Wang, S.B. Kang, Analytical investigation on catenary action in axially-restrained reinforced concrete beams, Eng. Struct. 192 (2019) 145–155.
[38] F.F. Feng, H.J. Hwang, S.M. Kang, W.J. Yi, Multilinear model for progressive collapse response of reinforced concrete frames under penultimate column removal scenario, J. Build. Eng. 47 (2022) 103850.
[39] N.S. Lim, K.H. Tan, C.K. Lee, A simplified model for alternate load path assessment in RC structures, Eng. Struct. 171 (2018) 696–711.
[40] A.T. Pham, K.H. Tan, Numerical investigations on static and dynamic responses of reinforced concrete sub-assemblages under progressive collapse, Eng. Struct. 149 (2017) 2–20.
[41] J. Yu, L. Luo, Y. Li, Numerical study of progressive collapse resistance of RC beam-slab substructures under perimeter column removal scenarios, Eng. Struct. 159 (2018) 14–27.
[42] D.C. Feng, G. Wu, Y. Lu, Numerical investigation on the progressive collapse behavior of precast reinforced concrete frame subassemblages, J. Perform. Constr. Facil. 32 (3) (2018) 04018027.

[43] Y.H. Weng, K. Qian, F. Fu, Q. Fang, Numerical investigation on load redistribution capacity of flat slab substructures to resist progressive collapse, J. Build. Eng. 29 (2020) 101109.
[44] G.Q. Chen, J.X. Lu, H. Wu, Dynamic behavior and retrofitting of RC frame building under vehicular bomb explosion, Eng. Fail. Anal. 143 (2023) 106925.
[45] R.R. Li, J. Yu, X.D. Zhou, M. Zhao, Analysis of progressive collapse process of RC structures based on hybrid framework of FEM-physics engine, Eng. Fail. Anal. 147 (2023) 107138.
[46] Fib, Fib Model Code for Concrete Structures 2010, Ernst & Sohn, 2013.
[47] Y.D. Murray, User Manual for LS-DYNA Concrete Material Model 159, Colorado: APTEK, Inc., 2007.
[48] B.A. Izzuddin, A.G. Vlassis, A.Y. Elghazouli, D.A. Nethercot, Progressive collapse of multi-storey buildings due to sudden column loss - part I: simplified assessment framework, Eng. Struct. 30 (5) (2008) 1308–1318.
[49] S.B. Kang, K.H. Tan, Progressive collapse resistance of precast concrete frames with discontinuous reinforcement in the joint, J. Struct. Eng. 143 (9) (2017) 04017090.
[50] K. Qian, Y.H. Weng, B. Li, Impact of two columns missing on dynamic response of RC flat slab structures, Eng. Struct. 177 (2018) 598–615.
[51] J. Yu, L.Z. Luo, Q. Fang, Structure behavior of reinforced concrete beam-slab assemblies subjected to perimeter middle column removal scenario, Eng. Struct. 208 (2020) 110336.
[52] Z. Yang, Y. Li, H. Guan, M.Z. Diao, B.P. Gilbert, H.L. Sun, L.W. Xu, Dynamic response and collapse resistance of RC flat plate structures subjected to instantaneous removal of an interior column, Eng. Struct. 264 (2022) 114469.
[53] A.T. Pham, K.H. Tan, Experimental study on dynamic responses of reinforced concrete frames under sudden column removal applying concentrated loading, Eng. Struct. 139 (2017) 31–45.